JACS
JOURNAL OF THE AMERICAN CHEMICAL SOCIETY
Article
pubs.acs.org/JACS

An Off–On COX-2-Specific Fluorescent Probe: Targeting the Golgi Apparatus of Cancer Cells

Hua Zhang,[†,§] Jiangli Fan,*[,†,§] Jingyun Wang,[‡] Shuangzhe Zhang,[†] Bairui Dou,[‡] and Xiaojun Peng*[,†,§]

[†]State Key Laboratory of Fine Chemicals and [‡]School of Life Science and Biotechnology, Dalian University of Technology, 2 Linggong Road, Hi-tech Zone, Dalian 116024, P.R. China

Supporting Information

ABSTRACT: Identifying cancer cells and quantifying cancer-related events in particular organelles in a rapid and sensitive fashion are important for early diagnosis and for studies on pathology and therapeutics of cancers. Herein a smart "off–on" cyclooxygenase-2-specific fluorescence probe (**ANQ-IMC-6**), able to report the presence of cancer cells and to image Golgi-related events, has been designed and evaluated. Cyclooxygenase-2 (COX-2) has been used as imaging target in the probe design, since this enzyme is a biomarker of virtually all cancer cell lines. In the free state in aqueous solution, **ANQ-IMC-6** mainly exists in a folded conformation where probe fluorescence is quenched through photoinduced electron transfer between the fluorophore acenaphtho[1,2-*b*]quinoxaline (ANQ) and the recognition group, indomethacin (IMC). Fluorescence is turned on, by restraining the photoinduced electron transfer, when **ANQ-IMC-6** is forced to adopt the unfolded state following binding to COX-2 in the Golgi apparatus of cancer cells. **ANQ-IMC-6** provides high signal-to-background staining and has been successfully used to rapidly differentiate cancer cells from normal cells when using flow cytometry and one- and two-photon fluorescence microscopic imaging. Furthermore, **ANQ-IMC-6** may be able to visualize dynamic changes of the Golgi apparatus during cancer cell apoptosis, with possible application to early diagnosis.

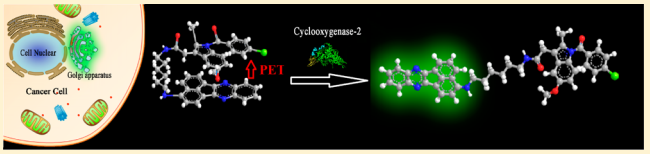

INTRODUCTION

Cancer is one of the major causes of death worldwide and in 2008 resulted in 7.6 million deaths (13% of the total).[1,2] Early diagnosis of cancer is particularly important for reducing cancer mortality.[2] In the past decade, molecular fluorescence microscopy imaging has come to offer opportunities for the early diagnosis of cancer due to its high selectivity, high resolution, and noninvasive capabilities.[3,4] In particular, molecular probes whose fluorescent signals are generated (off–on probes) by enzymic biomarkers of cancers hold great potential for identification and enumeration of living cancer cells.[5,6]

Recently, Urano et al.,[7] McCarley et al.,[8] and Marnett et al.[9,10] have designed fluorescent probes using overexpressed enzymes as imaging targets in the cancer cells. Thus γ-glutamyltranspeptidase (GGT), quinone oxidoreductase isozyme 1 (NQO1), and cyclooxygenase-2 (COX-2) have all been used to distinguish cancer cells from normal ones. These probes have widened our picture of possible molecular design ideas for the visualization of cancer cells. Regrettably, however, none of them could localize at and image single organelles of cancer cells. This limits their application for the study on the outcomes of therapy and for accurate and early diagnoses.

Consider the Golgi apparatus for instance. This organelle is a key structure for transporting and secreting some important proteins/enzymes which are overexpressed in cancer cells, for example COX-2. It has been suggested that when the stress-signaling threshold is exceeded, the Golgi apparatus automatically initiates apoptotic processes, which results in COX-2 accumulating in the Golgi apparatus.[11] Consequently, if the COX-2 in the Golgi apparatus of cancer cells could be visualized, then it might be possible to assess the efficacy of treatment protocols and the cellular impact of pharmaceutical targets, perhaps even permitting personalized oncology.[11]

It is in this context that we report a novel "off–on" COX-2-specific fluorescent probe, **ANQ-IMC-6** (Scheme 1), for rapid identification of cancer cells by imaging. This probe localizes in the Golgi apparatus and uses COX-2 as an imaging target. In aqueous buffer solution, **ANQ-IMC-6** is present in the folded state. This results in the quenching of fluorescence due to

Scheme 1. Chemical Structures of ANQ, IMC, and ANQ-IMC-6 (Folded and Unfolded)

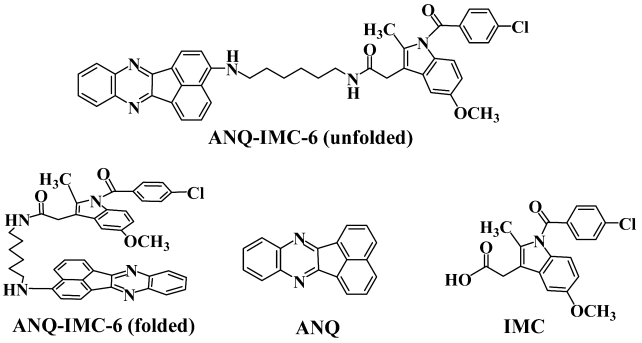

Received: June 7, 2013
Published: July 17, 2013

dx.doi.org/10.1021/ja4056905 | J. Am. Chem. Soc. 2013, 135, 11663–11669

photoinduced electron transfer (PET) between the acenaphtho[1,2-*b*]quinoxaline (ANQ, a fluorophore) and indomethacin (IMC, an inhibitor of COX-2). However intense fluorescence results from restraining PET following binding of **ANQ-IMC-6** to COX-2 in the Golgi apparatus. The probe exhibits a large Stokes shift (90 nm) due to the push−pull internal charge-transfer mechanism associated with the ANQ scaffold. In this way the probe's characteristics allow for the rapid, selective, and sensitive identification of cancer cells. As fluorescence intensity increase relates to the content of COX-2, **ANQ-IMC-6** may be of use for studying early cancer related and dynamic changes of the Golgi apparatus during cancer cells apoptosis, possibly facilitating early diagnoses.

RESULTS AND DISCUSSION

Design Strategy of Probe. For selective imaging of the Golgi apparatus of cancer cells, COX-2 was chosen as the imaging target because it is overexpressed in virtually all cancer cell lines and accumulates significantly in the Golgi apparatus.[9] ANQ was selected as the fluorophore, which results in **ANQ-IMC-6** displaying excellent fluorescence with two-photon features, such as increased penetration depth, localized excitation, and prolonged observation time.[12−15] The hexanediamine used as linker (Scheme 1) allows **ANQ-IMC-6** to exist in a folded conformation in aqueous solution. IMC, a good inhibitor for COX-2,[9,10] when linked to ANQ through hexanediamine acts as the binding-site for COX-2. Application of a molecular docking method (Figure S1a) indicates that **ANQ-IMC-6** binds to three amino acids of COX-2, i.e., Arg120, Tyr355, and Glu522, which is consistent with the known interaction of IMC with COX-2.[9,10]

The detailed synthetic route and chemical structure of **ANQ-IMC-6** are described in Scheme S1. The structures of **ANQ-IMC-6** and intermediates were well characterized by ^{1}H NMR, ^{13}C NMR, and TOF-MS (see Supporting Information text and Figure S1).

Spectral Properties and Discussion of Mechanism. The optical properties of **ANQ-IMC-6** were determined in Tris-HCl buffer (100 mM, pH 8.0). There was a significant fluorescence "off−on" process of **ANQ-IMC-6** when interacting with COX-2. When excited at 457 nm (ε = 16100 M^{-1} cm^{-1}), **ANQ-IMC-6** (2.0 μM) showed very weak fluorescence at 547 nm with Φ_F^{Free} 0.013. Upon binding to COX-2, it showed a 28-fold enhancement in fluorescence with $\Phi_F^{COX\text{-}2}$ 0.39 (Figure 1a). To elucidate the mechanism of the fluorescence "off−on" process, two conformations of **ANQ-IMC-6** (unfolded and folded, Scheme 1) were optimized, and their frontier molecular orbital (FMO) energies were calculated in water using Gaussian 09 (DFT/TDDFT in B3LYP/6-31G level). The calculated results show that in water the energy of the folded conformation is 3.0 kcal/mol lower than that of the unfolded conformation. The distance between two parallel planes of ANQ and IMC is about 0.36 nm. In this folded state, there is PET between ANQ and IMC. The oscillator strength from HOMO (S_0) to LUMO (S_1) is only 0.003, which means that electron transition from HOMO (S_0) to LUMO (S_1) is prohibited. Accordingly, the electronic transition from the excited state to the ground state cannot happen, and the fluorescence is quenched (Figure 2a). In the presence of COX-2, the binding of the IMC moiety to COX-2 could force the probe to adopt the unfolded conformation, because the hydrophobic cavity of COX-2 can only hold the IMC moiety. The hexanediamine linker is however long enough to enable

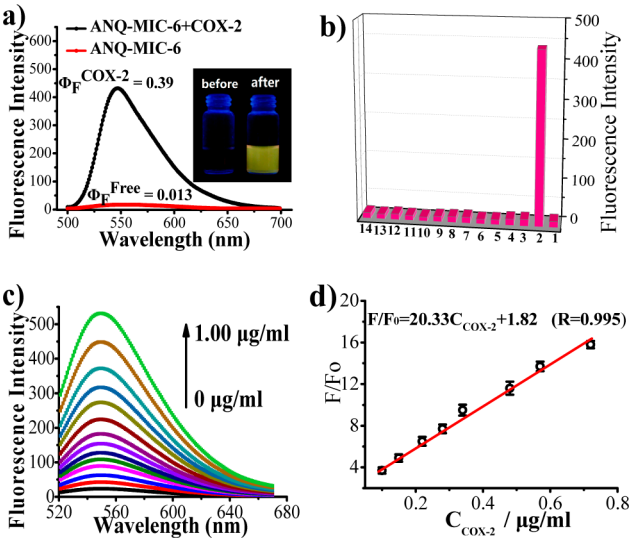

Figure 1. (a) Fluorescence emission spectra of **ANQ-IMC-6** (2.0 μM) in the absence and presence of COX-2 (0.50 μg/mL) in buffer at 25 °C. (b) Changes in fluorescence with different biomolecules (0.050 μg/mL) in buffer: 1, control; 2, COX-2; 3, RNA; 4, DNA; 5, triacylglycerol acylhydrolase; 6, lysozyme; 7, proteinase k; 8, histone; 9, collagen; 10, hemoglobin; 11, BSA; 12, β-amylase; 13, trypsin; and 14, chymotrypsin. (c) Emission spectra of **ANQ-IMC-6** (2.0 μM) upon the addition of increasing concentrations of COX-2 (0−1.0 μg/mL.) in buffer. (d) The fluorescence of **ANQ-IMC-6** (2.0 μM) related to COX-2 concentration (0.050−0.72 μg/mL). Condition: 100 mM Tris-HCl buffer (pH 8.0). The data are obtained from replicate experiments (n = 5).

the ANQ fluorophore moiety to extend into the large hydrophobic cavity of COX-2s' homodimer. These results were supported by a molecular docking method (Figure S1b−d). As a result of the unfolding, PET between ANQ and the IMC moieties does not occur, thus restoring fluorescence[16] (Figure 2b).

ANQ-IMC-6 did not exhibit observable fluorescence in the presence of various biomolecules, such as RNA, DNA, triacylglycerol acylhydrolase, BSA, and so on (Figure 1b). Furthermore, IC_{50}, 50% inhibiting concentration of **ANQ-IMC-6** for COX-2 was used to evaluate the binding capacity of **ANQ-IMC-6** for COX-2. The IC_{50} values of **ANQ-IMC-6** and IMC for COX-2 were 0.73 and 0.75 μM, respectively, indicating that the binding affinity of **ANQ-IMC-6** for COX-2 is as strong as that of IMC. Upon gradual addition of COX-2 to a solution of **ANQ-IMC-6**, the fluorescence intensity increased linearly with the COX-2 concentration over the range 0.12−0.72 μg/mL (Figure 1c,d). The detection limit for COX-2 was determined as 0.11 μg/mL (3σ/k), higher than the minimum expression of COX-2 (0.085 μg/mL) in cancer cells (Figure 1d),[17−19] demonstrating that **ANQ-IMC-6** could be used as a potential visual tool to selectively label cancer cells.

Verification for the Two-Photon Excitation Process of ANQ-IMC-6. That **ANQ-IMC-6** can undergo a two-photon excitation process was confirmed by a power dependence experiment. From the log−log plot of the emission intensity against incident power (Figure 3a), a linear regression with a slope of 2.06 was obtained, which indicates an obvious two-photon excitation process. As shown in Figure 3b, the activated two-photon action cross section $(\Phi\delta)_{max}$ of **ANQ-IMC-6** is 118 GM (1 GM = 10^{-50} cm^4 s/photon) when excited at 800 nm in the presence of COX-2 (0.50 μg/mL), and there was a 25-fold

dx.doi.org/10.1021/ja4056905 | J. Am. Chem. Soc. 2013, 135, 11663−11669

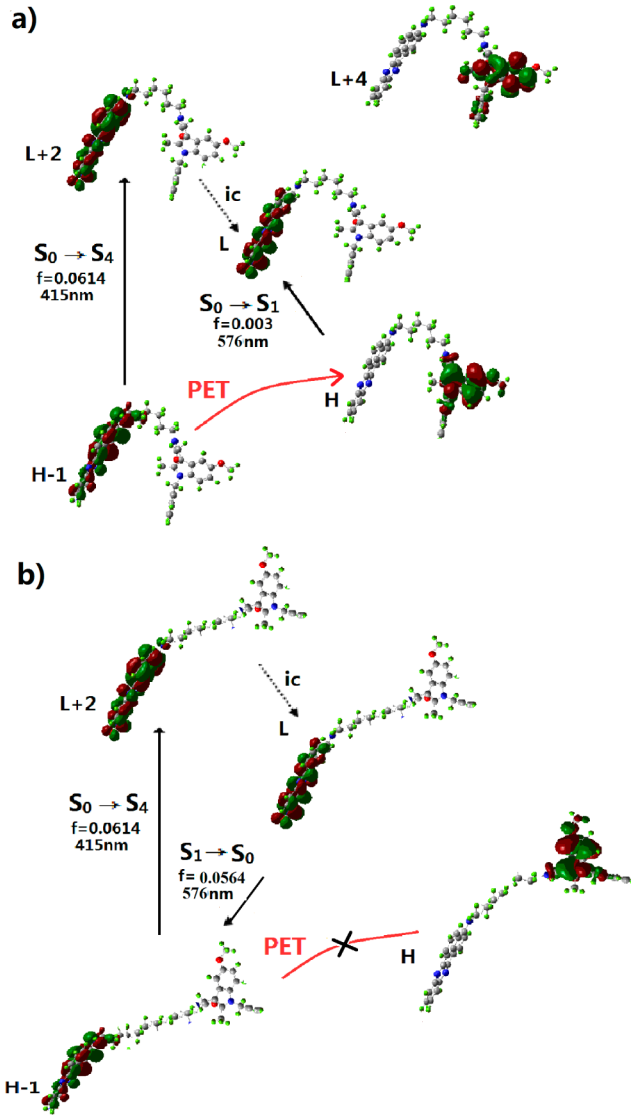

Figure 2. Structural optimization and FMO of **ANQ-IMC-6** (a) folded and (b) unfolded calculated with time-dependent DFT using Gaussian 09.

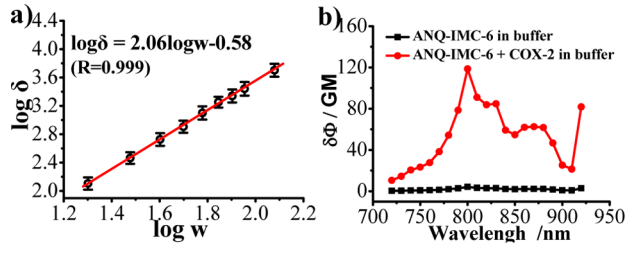

Figure 3. (a) The log–log plot of emission intensity against incident power. The linear regression equation is $\log \delta = 2.06 \log w - 0.58 (R = 0.999)$, where δ is the two-photon cross section, w the incident power, and R the correlation coefficient. (b) Two-photon action spectra of **ANQ-IMC-6** (2.0 μM) in the absence (black curve) and presence (red curve) of COX-2 (0.50 μg/mL) in buffer at 25 °C. Buffer: 100 mM Tris-HCl buffer (pH 8.0). Data are from replicate experiments (n = 5).

enhancement in the value $(\Phi\delta)_{max}$ compared with that seen in the absence of COX-2. These significant two-photon properties make **ANQ-IMC-6** suitable for two-photon microscopy imaging applications in living specimens.[20,21]

Selectively Imaging Living Cancer Cells. Before studying screening for living cancer cells by **ANQ-IMC-6**, enzyme linked immunosorbent assay (ELISA) was used to determine the amount of COX-2 in different cell lines. The data (Figure 4i) show that COX-2 was highly expressed in two cancer cell

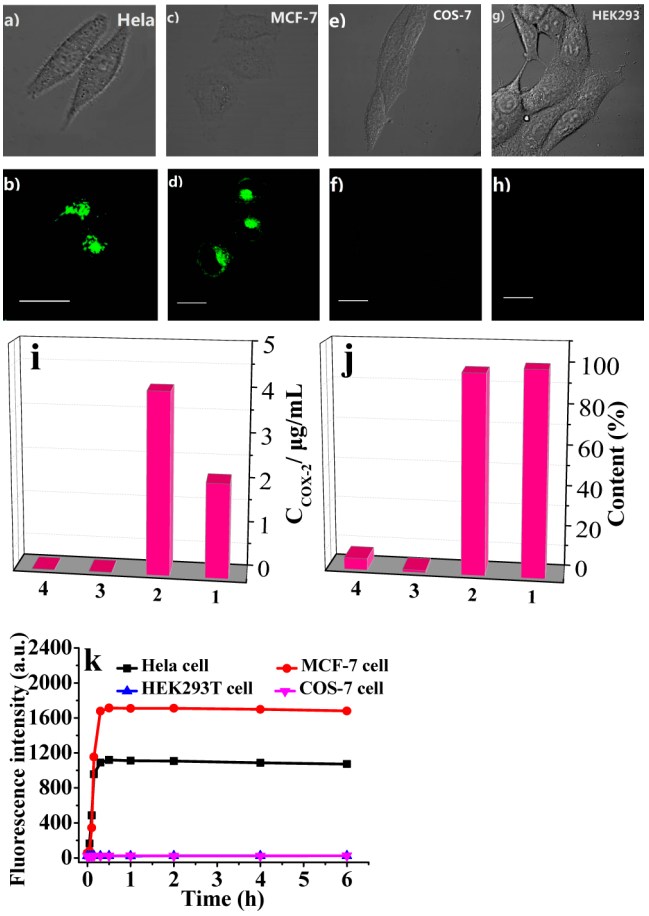

Figure 4. Living cells stained with **ANQ-IMC-6** (5.0 μM). (a, c, e, g) white light images and (b, d, f, h) fluorescence images. Excitation wavelength = 800 nm; scan range = 530–570 nm; and scale bar, 2.0 μm. (i) Quantification of COX-2 by ELISA (n = 5, p < 0.05). (j) FCM: 1, Hela cells; 2, MCF-7 cells; 3, COS-7 cells; 4, HEK 293 cells. (k) Response time of **ANQ-IMC-6** in MCF-7 cells. Images are representative of replicate experiments (n = 5).

lines (MCF-7 and Hela) but minimally expressed in two normal cell lines (COS-7 and HEK 293). Following this assay, the two cancer cell lines and two normal cell lines were incubated with **ANQ-IMC-6**. Upon excitation at 800 nm (TPM), both cancer cell lines showed strong and stable fluorescence after incubation for 30 min (Figure 4b and 4d), whereas both normal cell lines showed (Figure 4f and 4h) negligible fluorescence even after prolonged incubation (120 min). Similar results were obtained following excitation at 488 nm (OPM), see Figure S2. The fluorescent microscopy imaging results thus paralleled those seen with ELISA. All the results indicate that **ANQ-IMC-6** can distinguish cancer cells from normal cells by labeling overexpressed COX-2 in cancer cells.

Subsequently, flow cytometry (FCM) was used to evaluate the selectivity of **ANQ-IMC-6** for cancer cells on large cell populations. Histograms (Figure 4j) demonstrate that **ANQ-IMC-6** only stains cancer cells. Therefore, **ANQ-IMC-6** shows good applicability for the sorting of cancer cells in FCM.

dx.doi.org/10.1021/ja4056905 | J. Am. Chem. Soc. 2013, 135, 11663–11669

Furthermore, Figure 4k shows that **ANQ-IMC-6** strongly stained cancer cells within 0.5 h and that fluorescence intensity remained almost unchanged in cells for at least 6 h. Therefore, **ANQ-IMC-6** is suitable for long-term observations in living cancer cells.

Selective 3D Depth Imaging of Living Cancer Tissues. To further assess **ANQ-IMC-6** as a two-photon fluorescent probe for bioimaging applications, we investigated the applicability of this probe for tissue depth imaging. After incubation of liver tissue slices and sarcoma 180 tissue slices with 30 μM **ANQ-IMC-6** for 30 min at 37 °C, TPM images were obtained in the same region from 0 to 650 μm depth excited at 800 nm. Significantly, the sarcoma 180 tissue slices could be clearly visualized by green fluorescence at 50−550 μm depth (Figures 5b,c and S3). Only negligible fluorescence was observed in normal liver tissue slices.

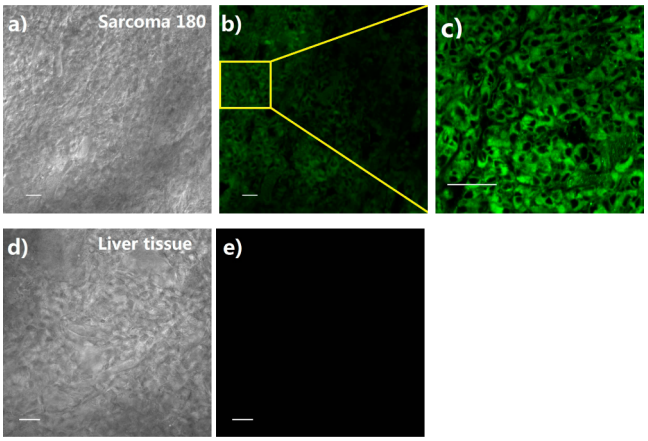

Figure 5. Living tissue slices stained with **ANQ-IMC-6** (30 μM). (a, d) white light images and (b, c, e) fluorescence images. Excitation wavelength = 800 nm; scan range = 530−570 nm; and scale bar, 5 μm. Images are representative of replicate experiments (n = 5).

Specific Localization of Golgi Apparatus of Cancer Cells. A well-known fluorescent probe for the Golgi apparatus, BODIPY TR C5-ceramide, was used to co-stain Hela cells with **ANQ-IMC-6** to determine its subcellular distribution. The co-localization coefficient was evaluated by Pearson's correlation factor.[22] Both the one photon fluorescence (OPM) (Figure 6a) and TPM (Figure 6b) images stained by **ANQ-IMC-6** match very well with those stained by BODIPY TR C5-ceramide (Figure 6c). The Pearson's correlation factor is 0.97 (Figure 6e), indicating that **ANQ-IMC-6** accumulates preferentially in the Golgi apparatus of this cancer cell line. The similar results (see Figure S4) were obtained in other cancer cell lines, such as Saos-2 (bone cancer), MDA-MB-468 (breast cancer), MKN-45(gastric cancer), Calu-3 (lung cancer), and HepG2 (liver cancer).

Furthermore, the log P value of **ANQ-IMC-6** (log P = 4.6) was estimated by using the Hansch and Leo procedure.[23] In QSAR model, log P = 3−5 should be required for retaining in Golgi.[24] So **ANQ-IMC-6** could enter into Golgi where it binds to COX-2.

The fluorescence intensity of **ANQ-IMC-6** remained >95% in solutions irradiated with an iodine-tungsten lamp for 7 h (Figure S5a) and >97% in cells after laser irradiation for 4 h (Figure S5b). MTT assay (Figure S6) revealed that 92% of HeLa cells survived after incubation with **ANQ-IMC-6** (6.0 μM) for 24 h. The two experiments indicate that **ANQ-IMC-6** possesses excellent photostability and very low cell toxicity.

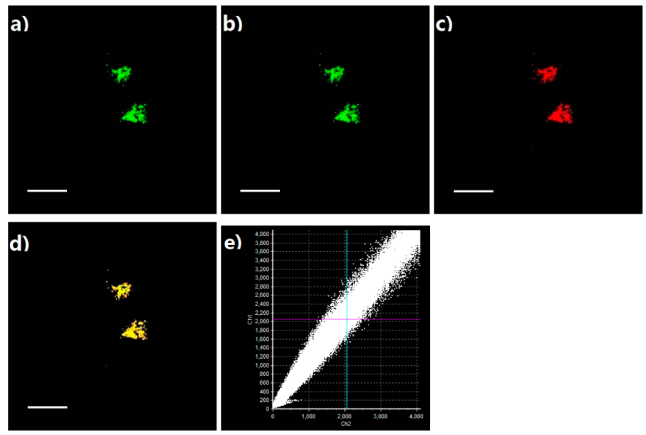

Figure 6. Fluorescence images of **ANQ-IMC-6** (5.0 μM) and BODIPY TR C5-ceramide (5.0 μM) in HeLa cells. (a, b) Stained with **ANQ-IMC-6**: (a) excitation wavelength = 800 nm, scan range = 530−570 nm; and (b) excitation wavelength = 488 nm, scan range = 530−570 nm. (c) Stained with BODIPY TR C5-ceramide, excitation wavelength = 543 nm, scan range = 600−640 nm. (d) Merged image of b and c. (e) Intensity correlation plot of stain **ANQ-IMC-6** and BODIPY TR C5-ceramide. Scale bar, 3.0 μm. Images and data are representative of replicate experiments (n = 5).

Imaging Morphological Changes of the Golgi Apparatus during the Cancers Cells Apoptosis. **ANQ-IMC-6** was used to visualize the dynamic morphological changes of the Golgi apparatus during the cancers cells apoptosis. As shown in Figure 7, **ANQ-IMC-6** stained the Golgi apparatus of MCF-7 cells with green fluorescence (Figure 7a−c). When further incubated with an apoptosis inducer, tea polyphenols, for 6 h,[25] the Golgi apparatus was fragmented and scattered near the nucleus (Figure 7d−f). The collapse is more extensive after 24 h (Figure 7g−i). The dynamic changes of cancer cells' Golgi apparatus observed during cancer cell apoptosis agree well with previous results obtained by scanning electron microscope (SEM),[26] providing a new mode of investigating diagnostically relevant changes in early stage cancer processes.

■ CONCLUDING REMARKS

We report a PET-quenched molecular probe (**ANQ-IMC-6**), a fluorogenic derivative of a COX-2 inhibitor, whose fluorescent signal is selectively and quickly generated by interaction with COX-2 accumulating in the Golgi apparatus of cancer cells. The "off−on" fluorescence enhancement results from restraining of PET following **ANQ-IMC-6** binding to COX-2 in the Golgi apparatus of cancer cell lines. The push−pull charge-transfer structure of **ANQ-IMC-6** provides significant two-photon properties permitting the selective identification of and screening for cancer cells. As a result, the probe permits rapid, highly selective and sensitive identification and enumeration of cancer cells in FCM and under traditional microscopy conditions via the imaging of Golgi apparatus of live cancer cells by normal and two-photon fluorescence microscopy. The two-photon system should be suitable for *in vivo* and *in vitro* thick-specimen imaging (50−550 μm), where the efficacy of treatment protocols and the cellular impact of pharmaceutical targets can be evaluated for personalized oncology. Moreover, **ANQ-IMC-6** also visualized dynamic

dx.doi.org/10.1021/ja4056905 | J. Am. Chem. Soc. 2013, 135, 11663−11669

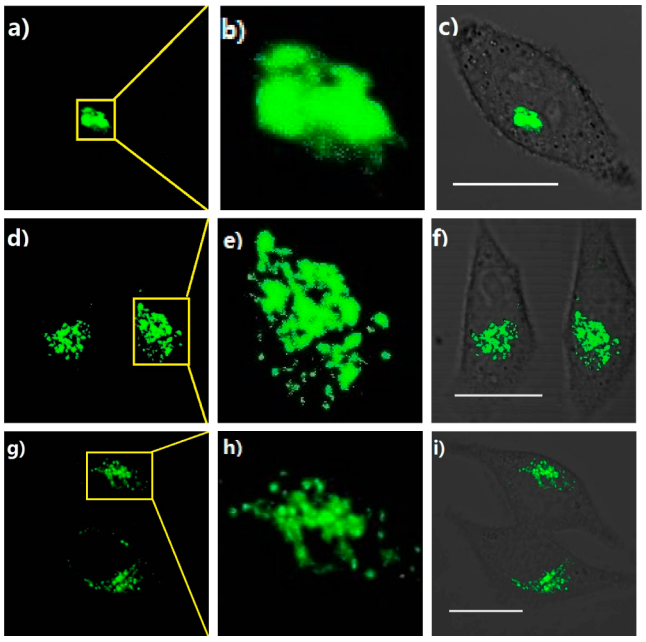

Figure 7. Changes in Golgi apparatus morphology of cancer cells during apoptosis. (a, b, d, e, g, h) Fluorescence images of MCF-7 cells stained with **ANQ-IMC-6** (5.0 μM). The concentration of tea polyphenols was 100 μM. Excitation wavelength = 800 nm, and scan range = 530−570 nm. (b, e, h) Amplifying images of a, d, and g. (c, f, i) Merged images of white light and fluorescence images. The incubation times of a, b, and c are 0 h, that of d, e, and f are 6 h, and that of g, h, and i are 24 h. Scale bar: 0.5 μm. Images are representative of replicate experiments (n = 5).

morphological changes of the Golgi apparatus during cancer cell apoptosis. We anticipate that **ANQ-IMC-6** could serve as a practical tool for the early diagnosis of cancers.

EXPERIMENTAL SECTION

COX-2-Targeted Fluorescent Agent Preparation. The preparation procedures of **ANQ-IMC-6** and related intermediates are given in the Supporting Information. All solvents and reagents used were reagent grade. Silica gel (100−200 mesh) was used for flash column chromatographic purification. BODIPY TR C5-ceramide was purchased from Life Technologies Co. (U.S.A.). Tris base was from Promega Co. (U.S.A.). COX-2 was obtained from Sigma Chemical Co. (U.S.A.). Doubly purified water used in all experiments was prepared using a Milli-Q system. The solutions of **ANQ-IMC-6** were typically prepared from 1.0 mM stock solutions in DMSO. Full details regarding materials, synthesis of compounds, and their characterization are described in the Supporting Information.

Mass spectral studies were carried out using a LC/Q-TOF mass spectrometer. An auto sampler operated in-line with a Quantum triple quadrupole instrument in ESI positive or negative ion mode. NMR spectra were obtained using a Varian Inova 400 MHz (or a Bruker Avance II 400 MHz) spectrometer. Experimental conditions included 2048 × 512 data matrix, 13 ppm sweep width, recycle delay of 1.5 and 4 scans per increment. The data were processed using squared sinebell window function, symmetrized, and displayed in magnitude mode.

Quantum Calculations. All the quantum chemical calculations were done with the Gaussian 09 suite.[27] The parameter referred to the work of Han.[28] The geometry optimizations of the dyes were performed using density functional theory (DFT)[29] with Becke's three-parameter hybrid exchange function with Lee−Yang−Parr gradient-corrected correlation functional (B3-LYP functional) and 6-31G ** basis set. No constraints to bonds/angles/dihedral angles were applied in the calculations, and all atoms were free to optimize. The electronic transition energies and corresponding oscillator strengths were calculated with time-dependent density functional theory (TD-DFT)[30,31] at the B3LYP/6-31G ** level.

Absorption and Fluorescence Quantum Yield Measurements. Absorption spectra were measured on a Lamda LS35 spectrophotometer. Fluorescence spectra were obtained with a FP-6500 spectrophotometer (Jasco, Japan). The relative fluorescence quantum yields were determined using Rhodamine B (Φ_F = 0.97 in methanol) as a standard[32] and calculated by the following equation:

$$\Phi_x = \Phi_s(F_x/F_s)(A_s/A_x)(\lambda_{exs}/\lambda_{exx})(n_x/n_s)^2$$

where Φ represents quantum yield; F is the integrated area under the corrected emission spectrum; A is absorbance at the excitation wavelength; λ_{ex} is the excitation wavelength; n is the refractive index of the solution (because of the low concentrations of the solutions, 10^{-7}−10^{-8} mol/L, the refractive indices of the solutions were replaced with those of the solvents); and the subscripts x and s refer to the unknown and the standard, respectively.

Measurement of Two-Photon Cross Section. The two-photon cross section (δ) was determined by using the femtosecond (fs) fluorescence measurement technique as described in the literature.[33] **ANQ-IMC-6** was dissolved in different solution at a concentration of 5.0×10^{-4} M, and then the two-photon induced fluorescence intensity was measured at 690−900 nm by using fluorescein (8.0×10^{-5} M, pH = 11.0) as the reference, whose two-photon properties of this dye are well characterized in the literature.[34] The intensities of the two-photon induced fluorescence spectra of the reference and sample resulting from the same excitation wavelength were determined. The TPA cross section was calculated by using equation:

$$\delta = \delta_r(S_s\Phi_r\varphi_r c_r)/(S_r\Phi_s\varphi_s c_s)$$

where the subscripts s and r stand for the sample and reference molecules. The intensity of the signal collected by a CCD detector was denoted as S. Φ is the fluorescence quantum yield, and φ is the overall fluorescence collection efficiency of the experimental apparatus. The number density of the molecules in solution was denoted as c. δ_r is the TPA cross section of the reference molecule. The measurements were performed as above while stirring the mixture with a small magnetic bar at 25 ± 0.5 °C. The data were obtained from replicate experiments (n = 5).

The figure is two-photon spectra, which was formed via the activated absorption cross-section ($\Phi\delta$) as y-axis and corresponding excitation wavelengths as x-axis. The two-photon spectra can show that the dyes have the highest two-photon absorption efficiency when excited at which wavelength.

Cell Culture and Staining with ANQ-IMC-6. HeLa, MCF-7, HEK293, COS-7, Saos-2, MDA-MB-468, MKN-45, Calu-3, and HepG2 cells were purchased from Institute of Basic Medical Sciences (IBMS) of the Chinese Academy of Medical Sciences. Cells were cultured for 3 days in phenol red-free Dulbecco's modified eagle's medium (DMEM, WelGene) supplemented with penicillin/streptomycin and 10% fetal bovine serum (FBS; Gibco) in a CO_2 incubator at 37 °C. One day before imaging, cells were seeded into a glass bottomed dish (MatTek, 35 mm dish with 20 mm well) and were incubated at 37 °C in a humidified incubator containing 5 wt % /vol CO_2. Before imaging, the live cells were incubated with 5.0 μM **ANQ-IMC-6** for 30 min at 37 °C under 5 wt % /vol CO_2 and then washed with phosphate-buffered saline (PBS) three times.

Preparation of Tissue Slices and Staining with ANQ-IMC-6. Tumor tissue slices were prepared from nude mice with S180 sarcoma. Normal tissue slices were prepared from livers of nude mice. The slices were cut at 700 μm using a vibrating-blade microtome in artificial cerebrospinal fluid (ACSF; 124 mM NaCl, 3 mM KCl, 26 mM $NaHCO_3$, 1.25 mM NaH_2PO_4, 10 mM D-glucose, 2.4 mM $CaCl_2$, and 1.3 mM $MgSO_4$). Slices were incubated with **ANQ-IMC-6** (30 μM) in ACSF bubbled with 95% O_2 and 5% CO_2 for 30 min at 37 °C and then washed three times with ACSF and transferred to a glass bottomed dish (MatTek, 35 mm dish with 20 mm well).

Two-Photon Fluorescence Imaging in the Cells and Tissues. Two-photon fluorescence imaging of **ANQ-IMC-6** in cells and tissues

dx.doi.org/10.1021/ja4056905 | J. Am. Chem. Soc. 2013, 135, 11663−11669

was obtained with a spectral confocal multiphoton microscope (Olympus, FV1000) with a high-performance mode-locked titanium-sapphire laser source (MaiTai, Spectra-Physics, U.S.A.). Numerical aperture (NA) was 1.43 and 1.30, respectively. The intensity images of **ANQ-IMC-6** were recorded with the emission in the range of 530−570 nm. To obtain images, internal PMTs were used to collect the signals in 8 bit unsigned 1024 × 1024 pixels at 400 Hz scan speed. Excitation wavelength: 800 nm. The images were obtained from replicate experiments (n = 5).

Live Cell Dual Staining with BODIPY FL C5-Ceramide. **ANQ-IMC-6** and BODIPY FL C5-Ceramide stock solutions were added to obtain 5.0 μM final concentrations. Cells were then incubated at 37 °C under 5 wt % /vol CO_2 for 30 min and then washed with phosphate-buffered saline (PBS) three times. Fluorescence imaging was then carried out with a spectral confocal one-photon microscope (Olympus, FV1000), using a 100× objective lens. Excitation wavelength: 488 nm. Green channel was collected at 530−570 nm, and red channel was collected at 600−640 nm. The images were obtained from replicate experiments (n = 5).

3D Depth Imaging in Tissues. Depth fluorescence imaging of **ANQ-IMC-6** in tissues was obtained with a spectral confocal multiphoton microscope (Olympus, FV1000) with a high-performance mode-locked titanium-sapphire laser source (MaiTai, Spectra-Physics, U.S.A.). The changes of fluorescence intensity with scan depth were determined by spectral confocal multiphoton microscopy (Olympus, FV1000) in the z-scan mode from 0 to 650 μm (step size = 3.0 μm).

Cytotoxicity. HeLa cells were prepared for cell viability studies in 96-well plates (1×10^5 cells per well that were incubated in 100 μL). The cells were incubated for an additional 20 h with dyes **ANQ-IMC-6**, NBD C6-Ceramide and BODIPY FLC5-Ceramide in different concentrations. Subsequently, 100 μL of 3-(4,5-dimethylthiazol-2-yl)-2,5-diphenyltetrazolium bromide (MTT, Sigma Chemical Co. U.S.A.) was added into each well, followed by further incubation for 24 h at 37 °C. The DMEM was remove and DMSO (200 μL/well) added to dissolve the reddish-blue crystals. Optical density (OD) was determined by a microplate reader (Spectra Max M5, Molecular Devices) at 570 nm with subtraction of the absorbance of the cell-free blank volume at 630 nm. The results from the six individual experiments were averaged. The relative cell viability (100%) was calculated using the following equation:

$$\text{cell viability}(\%) = (\text{OD}_{\text{dye}} - \text{OD}_{\text{K dye}})/(\text{OD}_{\text{control}} - \text{OD}_{\text{K control}}) \times 100$$

where dye stands for the sample containing **ANQ-IMC-6**, NBD C6-Ceramide, and BODIPY FLC5-Ceramide.

Flow Cytometry. HeLa, MCF-7, HEK293, and COS-7 cells were cultured in S6 RPMI 1640 supplemented with 10% FBS under an atmosphere of 5% CO_2 and 95% air at 37 °C. For FCM studies, macrophages in the exponential phase of growth were plated into 35 mm glass bottomed culture dishes (Φ 20 mm) containing 2.0 mL of RPMI 1640. After incubation at 37 °C with 5% CO_2 for 1−2 days to reach 70−90% confluency, the medium was removed. Then the cells were washed with 2.0 mL of PBS buffer, and 2.0 mL of fresh RPMI 1640 was added along with Lyso-NINO and/or iNOS stimulants. Cells were incubated for 12 h prior to FCM analysis. Samples were illuminated with a sapphire laser at 488 nm on a FACScan flowcytometer (BD Biosciences Pharmingen, U.S.A.). The fluorescence of the forward- and side-scattered light from 10 000 cells was detected at rate of 150 events/second. FCM data were analyzed with FACSDiva software.

ELISA for the Determination of COX-2. This assay used the ABC-double antibody sandwich ELISA method. COX-2 kit (human, double antibody method, 96t) was purchased from CBS. Cells and tissues were prepared as homogenates and preserved at 2−8 °C. The ELISA assay experiment was carried out according to literature procedures.[9]

Estimation of Log P and Use of QSAR Model for Predicting Probe Localization. The log P (logarithm of the octanol−water partition coefficient) value of **ANQ-IMC-6** was estimated using the procedures described by Hansch and Leo. The predicted membrane permeability and intracellular localizations for these species were assessed by appropriate quantitative structure activity relations models by methods described in the literature.

■ ASSOCIATED CONTENT

Ⓢ Supporting Information

Synthetic protocol and characterization data for **ANQ-IMC-6**; living cell imaging by OPM; 3D depth imaging in tissue; photostability in solution and cell. This material is available free of charge via the Internet at http://pubs.acs.org.

■ AUTHOR INFORMATION

Corresponding Author

fanjl@dlut.edu.cn; pengxj@dlut.edu.cn

Author Contributions

[§]These authors contributed equally.

Notes

The authors declare no competing financial interest.

■ ACKNOWLEDGMENTS

This work was financially supported by the National Science Foundation of China (21136002, 20923006, and 21076032), National Basic Research Program of China (2009CB724706 and 2013CB733702), National High Technology Research and Development Program of China (863 Program, 2011AA02A105) and Ministry of Education (NCET-12-0080).

■ REFERENCES

(1) Jemal, A.; Siegel, R.; Xu, J.; Ward, E. *Cancer. J. Clin.* **2010**, *60*, 277−300.

(2) For more detailed information see the website: http://www.who.int/gho/ncd/mortality_morbidity/cancer/en/index.html; http://www.who.int/topics/cancer/en/index.html.

(3) Helmchen, F.; Denk, W. *Nat Methods* **2005**, *2*, 932−935.

(4) Samuel, T. H.; Thanu, P. K.; Michael, D. M. *Biophys. J.* **2006**, *91*, 4258−4272.

(5) Siegel, R.; Naishadham, D.; Jemal, A. *Ca-Cancer J. Clin.* **2012**, *62*, 10−29.

(6) Nguyen, Q. T.; Olson, E. S.; Aguilera, T. A.; Jiang, T.; Scadeng, M.; Ellies, L. G.; Tsien, R. Y. *Proc. Natl. Acad. Sci. U.S.A.* **2010**, *107*, 4317−4322.

(7) Urano, Y.; Sakabe, M.; Kosaka, N.; Ogawa, M.; Mitsunaga, M.; Asanuma, D.; Kamiya, M.; Young, M. R.; Nagano, T.; Choyke, P. L.; Kobayashi, H. *Sci. Transl. Med.* **2011**, *3*, 110−119.

(8) William, S. C.; Prasai, B.; Burk, D. H.; Brown, M. L.; McCarley, R. L. *J. Am. Chem. Soc.* **2013**, *135*, 309−314.

(9) Uddin, M. J.; Crews, B. C.; Blobaum, A. L.; Kingsley, P. J.; Gorden, D. L.; McIntyre, J. O.; Matrisian, L. M.; Subbaramaiah, K.; Dannenberg, A. J.; Piston, D. W.; Marnett, L. J. *Cancer Res.* **2010**, *70*, 3618−3627.

(10) Uddin, M. J.; Crews, B. C.; Ghebreselasie, K.; Marnett, L. J. *Bioconjugate Chem.* **2013**, *24*, 712−723.

(11) Wlodkowic, D.; Skommer, J.; McGuinness, D.; Hillier, C.; Darzynkiewicz, Z. *Leuk. Res.* **2009**, *33*, 1440−1447.

(12) Chen, T.; Wang, X. H.; Wangenheim, D.; Zheng, M. Z.; Samaj, J.; Ji, W. Q.; Lin, J. X. *Protoplasma* **2012**, *249*, 1183−1183.

(13) Bai, S. J.; Fabian, T.; Prinz, F. B.; Fasching, R. J. *Sens. Actuators, B* **2008**, *130*, 249−257.

(14) Zipfel, W. R.; Williams, R. M.; Webb, W. W. *Nat. Biotechnol.* **2003**, *21*, 1369−1377.

(15) Helmchen, F.; Denk, W. *Nat. Methods* **2005**, *2*, 932−940.

(16) Zhang, X.; Wu, Y. B.; Ji, S. M.; Guo, H. M.; Song, P.; Han, K. L.; Wu, W. T.; Wu, W. H.; James, T. D.; Zhao, J. Z. *J. Org. Chem.* **2010**, *75*, 2578−2588.

(17) Denkert, C. *Cancer* **2003**, *97*, 2978−2987.

(18) Sung, Y. K. *Mol. Cells* **2004**, *17*, 35−38.
(19) Mrena, J. *Tumor Biol.* **2010**, *31*, 1−7.
(20) Xu, C.; Zipfel, W.; Shear, J. B.; Williams, R. M.; Webb, W. W. *Proc. Natl. Acad. Sci. U.S.A.* **1996**, *93*, 10763−10768.
(21) Xu, C.; Webb, W. W. *J. Opt. Soc. Am. B* **1996**, *13*, 481−491.
(22) Li, Q.; Lau, A.; Morris, T. J.; Guo, L.; Fordyce, C. B.; Stanley, E. J. *Neuroscience* **2004**, *24*, 4070−4081.
(23) Hansch, C.; Leo, A. *Substituent constants for correlation analysis in chemistry and biology*; Wiley: New York, 1979; pp 18−43.
(24) Horobin, R. W.; Rashid, D. F. *Biotech. Histochem.* **2013**, DOI: 10.3109/10520295.2013.780635.
(25) Yu, J.; Zhang, L.; Hwang, M. P.; Kinzler, K. W.; Vogelstein, B. *Mol. Cell* **2001**, *7*, 673−682.
(26) Kellokumpua, S.; Sormunenb, R.; Kellokumpu, I. *FEBS Lett.* **2002**, *516*, 217−224.
(27) Frisch, M. J.; Trucks, G. W.; Schlegel, H. B.; Scuseria, G. E.; Robb, M. A.; Cheeseman, J. R.; Scalmani, G.; Barone, V.; Mennucci, B.; Petersson, G. A.; Nakatsuji, H.; Caricato, M.; Li, X.; Hratchian, H. P.; Izmaylov, A. F.; Bloino, J.; Zheng, G.; Sonnenberg, J. L.; Hada, M.; Ehara, M.; Toyota, K.; Fukuda, R.; Hasegawa, J.; Ishida, M.; Nakajima, T.; Honda, Y.; Kitao, O.; Nakai, H.; Vreven, T.; Montgomery, J. A., Jr.; Peralta, J. E.; Ogliaro, F.; Bearpark, M.; Heyd, J. J.; Brothers, E.; Kudin, K. N.; Staroverov, V. N.; Kobayashi, R.; Normand, J.; Raghavachari, K.; Rendell, A.; Burant, J. C.; Iyengar, S. S.; Tomasi, J.; Cossi, M.; Rega, N.; Millam, J. M.; Klene, M.; Knox, J. E.; Cross, J. B.; Bakken, V.; Adamo, C.; Jaramillo, J.; Gomperts, R.; Stratmann, R. E.; Yazyev, O.; Austin, A. J.; Cammi, R.; Pomelli, C.; Ochterski, J. W.; Martin, R. L.; Morokuma, K.; Zakrzewski, V. G.; Voth, G. A.; Salvador, P.; Dannenberg, J. J.; Dapprich, S.; Daniels, A. D.; Farkas, Ö.; Foresman, J. B.; Ortiz, J. V.; Cioslowski, J.; Fox, D. J. *Gaussian 09*, revision A.02; Gaussian, Inc.: Wallingford, CT, 2009.
(28) Zhou, L. C.; Zhao, G. J.; Liu, J. F.; Han, K. L.; Wu, Y. K.; Peng, X. J.; Sun, M. T. *J. Photochem. Photobiol., A* **2007**, *187*, 305−310.
(29) Dreizler, M. R.; Gross, E. K. U. *Density Functional Theory*; Springer Verlag: Heidelberg, 1990.
(30) Gross, E. K. U.; Kohn, W. *Phys. Rev. Lett.* **1985**, *55*, 2850−2852.
(31) Stratmann, R. E.; Scuseria, G. E.; Frisch, M. J. J. *Chem. Phys.* **1998**, *109*, 8218−8224.
(32) Velapoldi, R. A.; T€onnesen, H. H. *J. Fluoresc.* **2004**, *14*, 465−472.
(33) Lee, S. K.; Yang, W. J.; Choi, J. J.; Kim, C. H.; Jeon, S. J.; Cho, B. R. *Org. Lett.* **2005**, *7*, 323−326.
(34) Xu, C.; Webb, W. W. *J. Opt. Soc. Am. B* **1996**, *13*, 481−489.